Biosensors and Bioelectronics 87 (2017) 998–1004

Contents lists available at ScienceDirect

Biosensors and Bioelectronics

journal homepage: www.elsevier.com/locate/bios

Nanostructured cobalt phosphates as excellent biomimetic enzymes to sensitively detect superoxide anions released from living cells

Min-Qiang Wang[a], Cui Ye[b], Shu-Juan Bao[a,*], Mao-Wen Xu[a], Yan Zhang[a], Ling Wang[a], Xiao-Qing Ma[a], Jun Guo[c], Chang-Ming Li[a]

[a] Institute for Clean Energy & Advanced Materials, Faculty of Materials and Energy, Southwest University, Chongqing 400715, PR China
[b] Key Laboratory of Eco-environments in Three Gorges Reservoir Region (Ministry of Education), School of Chemistry and Chemical Engineering, Southwest University, Chongqing 400715, PR China
[c] Analysis and test center of Suzhou University, Jiangsu 215000, PR China

ARTICLE INFO

Keywords:
Cobalt phosphate
Biomimetic enzymes
Superoxide anion radical
Biosensor

ABSTRACT

Monitoring superoxide anion radicals in living cells has been attracting much academic and industrial interest due to the dual roles of the radicals. Herein, we synthesized a novel nanostructured cobalt phosphate nanorods ($Co_3(PO_4)_2$ NRs) with tunable pore structure using a simple and effective micro-emulsion method and explored their potential utilization in the electrochemical sensing of superoxide anions. As an analytical and sensing platform, the nanoscale biomimetic enzymes $Co_3(PO_4)_2$ NRs exhibited excellent selectivity and sensitivity towards superoxide anion ($O_2^{\bullet -}$) with a low detection limit (2.25 nM), wide linear range (5.76–5396 nM), and long-term stability. Further, the nanoscale biomimetic enzyme could be efficiently applied in situ to electrochemically detect $O_2^{\bullet -}$ released from human malignant melanoma cells and normal keratinocyte, showing excellent real time quantitative detection capability. This material open up exciting opportunities for implementing biomimetic enzymes in nanoscale transition metal phosphates and designing enzyme-free biosensors with much higher sensitivity and durability in health and disease analysis than those of natural one.

1. Introduction

It is well known that superoxide anions ($O_2^{\bullet -}$) is a typical type of reactive oxygen species (ROS), which not only serves as a precursor of other ROS, such as a hydroxyl radical (•OH), hydrogen peroxide (H_2O_2), et al., but also can inactivate nitric oxide (NO), thereby causing endothelial dysfunction (Ahmad et al., 2015; Fitzgerald et al., 2015; Long et al., 2015; Wang et al., 2016b). Under normal physiological conditions, $O_2^{\bullet -}$ plays an important role as a regulatory mediator in signaling processes. Excessive accumulation of $O_2^{\bullet -}$ may cause damage to biological membranes, tissues, and organisms (Zhou et al., 2016). Thus, it is of great importance to detect $O_2^{\bullet -}$ quickly, reliably, sensitively, and specifically for pathological study, disease diagnosis, and health screening. Nevertheless, due to great differences in chemical properties of various ROS (such as half-life, reactivity, and compartmental distribution) and biochemical complexity of cellular milieu, specific detection of single ROS in living cells and tissues would be beneficial for clarifying the controversial effects of a specific ROS in biological phenomena. Throughout the past few decades, a great deal of effort has been devoted to exploring reliable $O_2^{\bullet -}$ sensing techniques, such as electron spin resonance trapping, spectrophotometry, chemiluminescence, chromatograph, and fluorescence (Diez et al., 2001; Ohara et al., 1993; Vásquez-Vivar et al., 1998; Zhang et al., 2005; Zweier et al., 1987). In addition to these techniques, electrochemical methods have received extensive attention owing to their intrinsic advantages including direct and real-time detection, high sensitivity, facile operation, possibility of in vivo detection and so on (Ignatov et al., 2002). Recently, the effective electrochemical sensing of $O_2^{\bullet -}$ mainly based on the incorporation of enzymes like superoxide dismutase (SOD) onto electrodes has been extensively employed due to its good selectivity and sensitivity (Di et al., 2004; Tian et al., 2002). Nevertheless, the enzyme-based biosensors suffer from relatively high cost, short lifetime, poor reproducibility, and the critical operating situation (Dai et al., 2009; Wang et al., 2016a). Therefore, synthetic biomimetic enzyme is an alternative to detect $O_2^{\bullet -}$ by its catalytic dismutation of $O_2^{\bullet -}$ as a low cost artificial enzyme while possessing excellent stability.

In recent years, nanomaterials have attracted much interest for their potential use in nanomedicine and electrochemical fields. Moreover, the strong biomimetic electrocatalytic activity exhibited by some nanoparticles has introduced exciting possibilities to develop novel ultrasensitive and high-selective enzyme free biosensors with

* Corresponding author.

http://dx.doi.org/10.1016/j.bios.2016.09.066
Received 13 August 2016; Received in revised form 12 September 2016; Accepted 19 September 2016
Available online 20 September 2016
0956-5663/ © 2016 Elsevier B.V. All rights reserved.

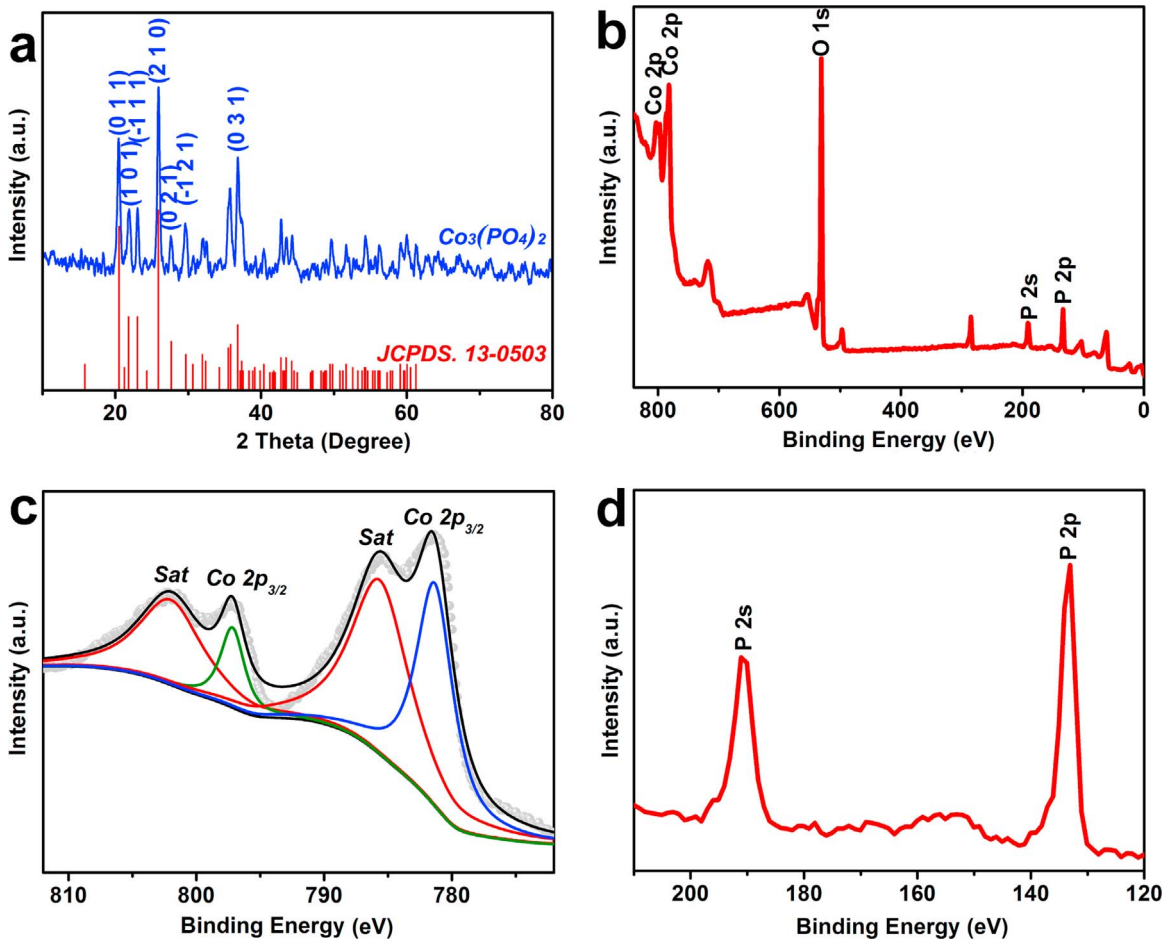

Fig. 1. (a) Experimental and simulated XRD patterns of as-prepared $Co_3(PO_4)_2$ NRs. (b) XPS analysis about (b) wide scan survey spectra of $Co_3(PO_4)_2$ NRs, (c) Co 2p spectra in $Co_3(PO_4)_2$ NRs, (d) P 2s and P 2p spectra in $Co_3(PO_4)_2$ NRs.

enhanced stability (Ye et al., 2015). As an important inorganic function materials, phosphates are present throughout the body and are regarded as biocompatible biomaterials (Barnese et al., 2008); Meanwhile, cobalt complexes have been described as superoxide dismutase biomimetic enzymes (Anacona et al., 2003; Durot et al., 2005; Pierre et al., 1995; Salvemini et al., 2002). Additionally , transition metal phosphates have been of pivotal importance in material sciences because of their unique catalytic and electronic properties compared to their oxide counterparts (Cheetham et al., 1999), and their promising capabilities have been widely demonstrated in various areas, including catalysis, optoelectronics, energy conversion and storage, and biological platforms (Arico et al., 2005; Garrou, 1985; Hu et al., 2015; Knowles, 2003). The development of nanoscience and nanotechnology has led to the discovery that the combination of low dimensionality and well-defined nanostructures may let various function materials exhibit even more attractive features (Liao et al., 2016). However, traditional synthetic strategies for cobalt phosphate are often performed with solution chemistry or solid state reactions, resulting in products with limited size and surface area rather than with nanoscale dimensions, which is more desirable for various applications (Feng et al., 1997; Natarajan et al., 2000).

Micro-emulsion is a thermodynamically stable system consisting of two or more immiscible liquids (Tilley et al., 2005). In the micro-emulsions, not only the small size and shape can be precisely controlled, but the better size distribution can also be obtained. Due to the ability to obtain uniformed fine particles, micro-emulsion method exhibit great potential in fabricating nanoscale materials, such as molybdenum sulfide, silica/cadmium sulfide nanometer composites and AgBr (Boakye et al., 1994; Entezari and Ghows, 2011; Husein et al., 2007). However, the preparation of nanoscale cobalt phosphate with the micro-emulsion method has not yet been successful. Herein, we report on the preparation of nanoscale cobalt phosphate via micro-emulsion method for the first time. Using the cobalt phosphate as biomimetic enzymes, a superoxide anion electrochemical analysis platforms was developed for ultrasensitive and selective detection of $O_2^{\bullet-}$. Due to the low detection limit, high sensitivity, and excellent selectivity, the prepared $Co_3(PO_4)_2$ NRs based biosensor exhibited ultrasensitive detection of $O_2^{\bullet-}$ released from living normal and cancer cells.

2. Experimental section

2.1. Materials

Analytical grade cobalt chloride hexahydrate ($CoCl_2{\cdot}6H_2O$) and potassium phosphate (K_3PO_4) were obtained from Sinopharm Chemical Reagent Co., SDBS, isooctane (C_8H_{18}), and n-butyl alcohol ($C_4H_{10}O$) were purchased from Aladdin Industrial Co., (Shanghai, China). Potassium superoxide (KO_2), Zymosan A (Zym, from Saccharomyces cerevisiae), SOD (from bovine erythrocytes), 0.01 M pH 7.4 Phosphate buffer solution (PBS), and Nafion (5 wt%) were obtained from Sigma-Aldrich. The $O_2^{\bullet-}$ solutions were prepared by the addition of KO_2 solid powder to PBS (N_2 saturated). Hacat (spontaneously immortalized human keratinocyte) and A375 (human malignant melanoma cells) cell lines were obtained from Southwest University, and cultured in a humidified incubator (95% air with 5% CO_2) at 37 °C. The concentration of $O_2^{\bullet-}$ was determined by recording the reduction of ferri cytochrome c spectrophotometrically and using

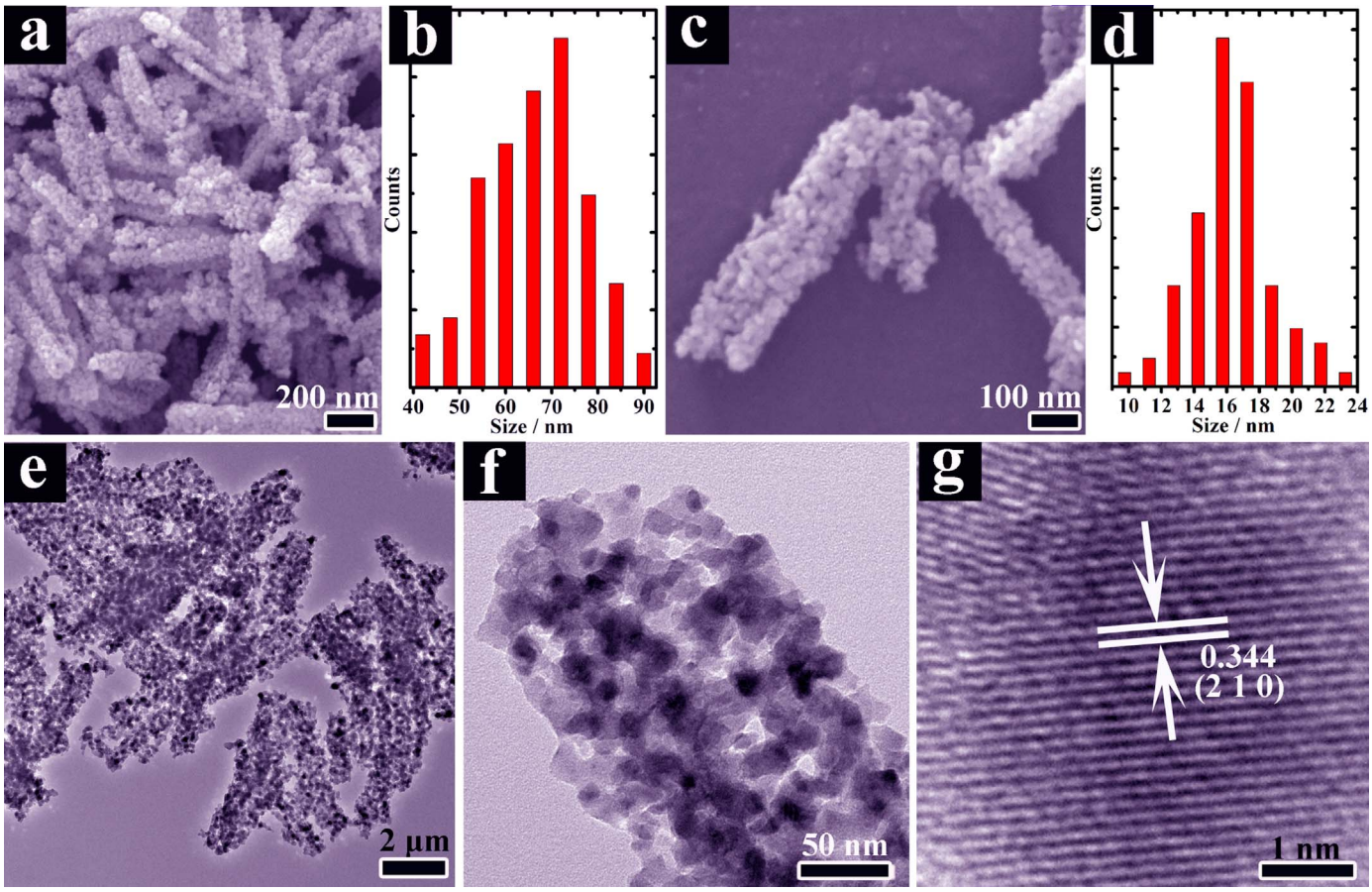

Fig. 2. (a, c) FESEM images of $Co_3(PO_4)_2$ nanorods. Size distributions for (b) diameter and (d) nanoparticle of $Co_3(PO_4)_2$ nanorods. (e and f) TEM and (g) HRTEM of $Co_3(PO_4)_2$ nanorods.

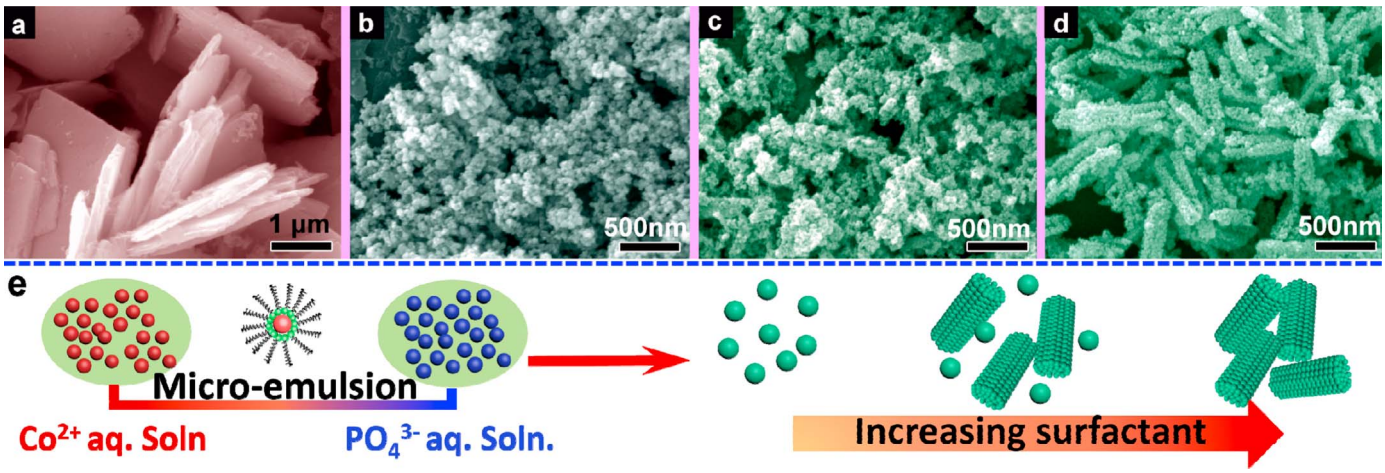

Fig. 3. (a) FESEM images of $Co_3(PO_4)_2$ sheets that obtained in aqueous solution. Varying the dosage of surfactant and the other condition remain in unchanged: (b) 1.1 g. (c) 2.2 g. (d) 3.3 g. (e) The schematic illustration of the formation of $Co_3(PO_4)_2$ nanorods.

the extinction coefficient (21.1 mM^{-1} cm^{-1}) of ferrocytochrome c at 550 nm The other chemicals were purchased from Sigma-Aldrich and used without further purification. Deionized water (18.2 MX) was used throughout the experiments.

2.2. Preparation of the bulk $Co_3(PO_4)_2$ in aqueous solution

6 mL aqueous solution of $CoCl_2{\cdot}6H_2O$ (0.45 mol L^{-1}) was added to 6 mL aqueous solution of K_3PO_4 (0.3 mol L^{-1}), After the deposition reaction finished, the mixture were washed via centrifugation at 8000 rpm for 5 min with ethanol and deionized water for several times and then dried under vacuum at 60 °C. Further annealed with a rising rate of 5 °C min^{-1} to 650 °C and kept for 3 h to remove the crystal water and form bulk $Co_3(PO_4)_2$.

2.3. Preparation of the nanoscale $Co_3(PO_4)_2$ NRs

Water in oil type of SDBS-C_8H_{18}-$C_4H_{10}O$-H_2O micro-emulsion was used as reaction system because of its high water/oil ratio and abundant phase diagram date. SDBS is a surfactant, C_8H_{18} is an oil

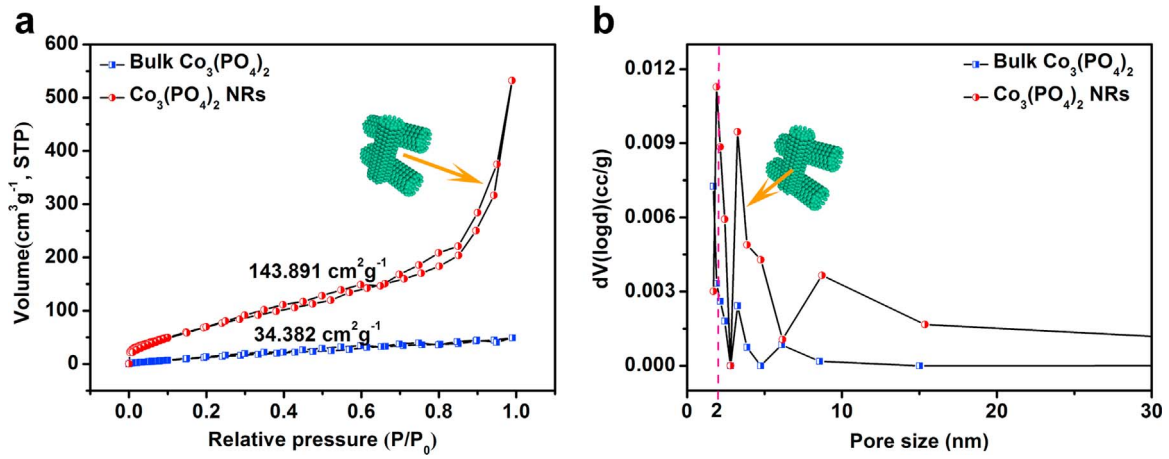

Fig. 4. (a) Nitrogen adsorption-desorption of the prepared bulk $Co_3(PO_4)_2$ and $Co_3(PO_4)_2$ NRs. (b) Pore-size distribution isotherms of the prepared bulk $Co_3(PO_4)_2$ and $Co_3(PO_4)_2$ NRs.

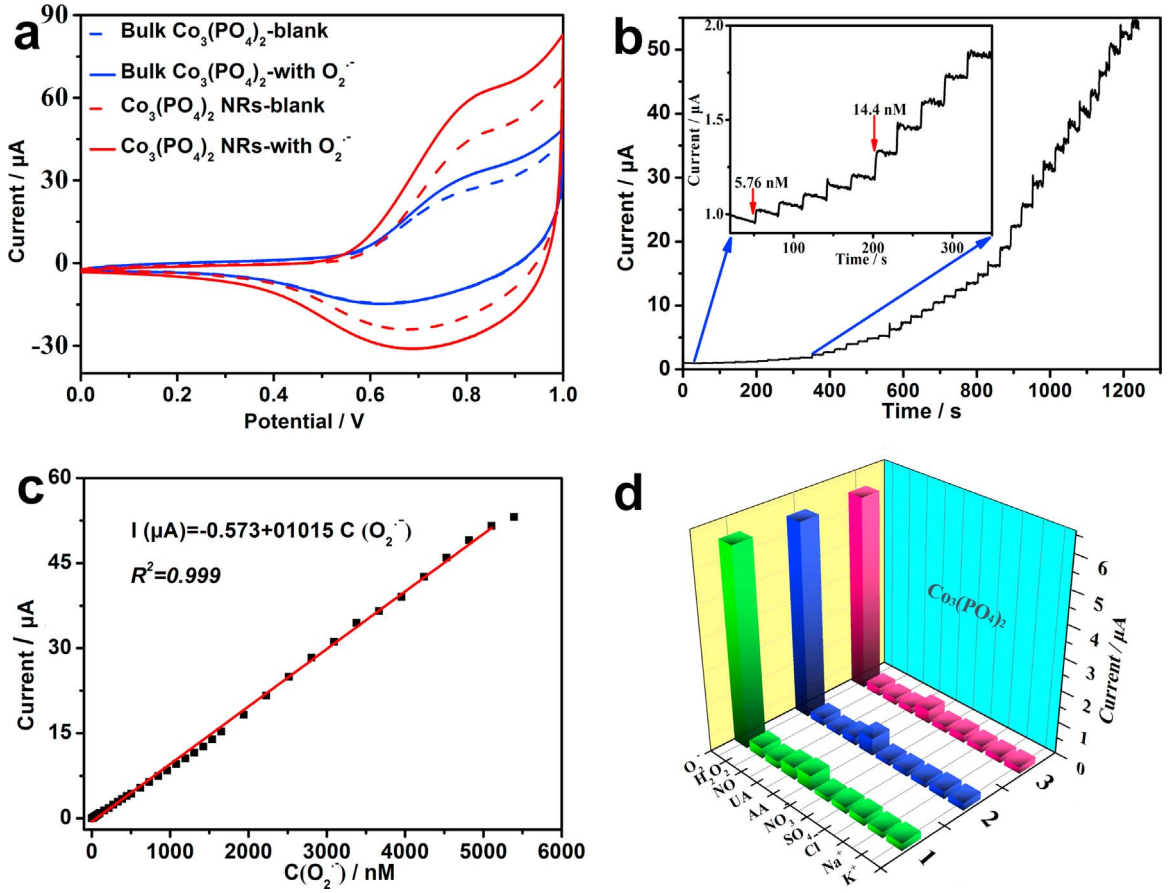

Fig. 5. (a) Cyclic voltammetry curves (CVs) of the prepared bulk $Co_3(PO_4)_2$ and prepared $Co_3(PO_4)_2$ NRs based electrodes in the absence (dotted line) and presence (solid line) of $O_2^{\cdot-}$. (b) Chronoamperometric response and (c) linear calibration curve of $Co_3(PO_4)_2$ NRs/GC electrode sensors upon continuous injection of different concentration $O_2^{\cdot-}$ at an applied potential of 0.7 V in 0.01 M pH 7.4 PBS. (d) Selectivity and reproducibility of the $Co_3(PO_4)_2$ NRs/GC electrode sensors when analyzed with K^+, Na^+, Cl^-, SO_4^{2-}, NO_3^-, AA, UA, NO, H_2O_2, and $O_2^{\cdot-}$.

phase, $C_4H_{10}O$ is a cosurfactant. $CoCl_2{\cdot}6H_2O$ or K_3PO_4 aqueous solution is an aqueous phase, respectively.

6 mL aqueous solution of $CoCl_2{\cdot}6H_2O$ (0.45 mol L^{-1}) was added to the mixture of SDBS (3.3*g*), C_8H_{18} (36 mL), and $C_4H_{10}O$ (12 mL) under ultrasound for 15 min at room temperature to construct the micro-emulsion system. Next, 6 mL aqueous solution of K_3PO_4 (0.3 mol L^{-1}) was further added in the above micro-emulsion system slowly in 2 min under ultrasound for 30 min at room temperature by syringe. After the deposition reaction finished, the mixture were washed via centrifugation at 8000 rpm for 5 min with ethanol and deionized water for several times and then dried under vacuum at 60 °C. Further annealed with a rising rate of 5 °C min^{-1} to 650 °C and kept for 3 h to remove the crystal water and form $Co_3(PO_4)_2$ NRs.

2.4. Preparation of modified electrodes

Glassy carbon electrode (GCE, d=3 mm) was respectively polished with 0.3 and 0.05 μm alumina slurry followed by rinsing thoroughly with double distilled water, and then ultrasonically cleaned in ethanol and double distilled water to obtain a mirror-like surface. The electro-

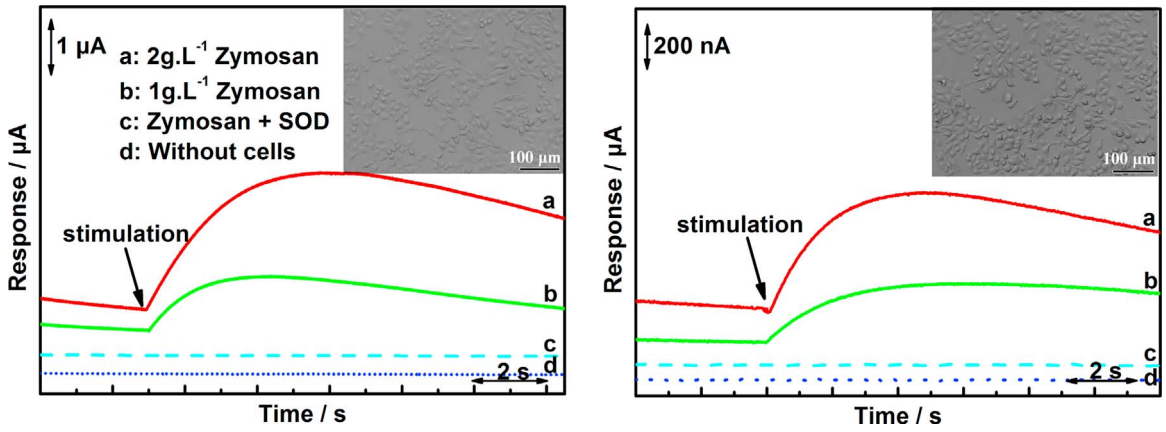

Fig. 6. Real time monitoring of $O_2^{\bullet-}$ released from (a) HaCat cells and (b) A375 cells (inset of the cell images with the density of 5×10^4) stimulated by different amount of Zymosan in cell culture medium, (curve a) 2 g L^{-1} Zymosan; (curve b) 1 g L^{-1} Zymosan; (curve c) 1 g L^{-1} Zymosan and SOD 300 U mL^{-1}; and (curve d) without cells.

des were then electrochemically characterize by potential cycling in KCl containing solution 5 mmol $K_3[Fe(CN)_6]$ in a potential range over −0.1–0.6 V at a scan rate of 50 mV s^{-1} until a typical cyclic voltammogram (less than 80 mV peak potential differences) characteristic of a clean GCE electrode was obtained. The as-prepared $Co_3(PO_4)_2$ NRs (5 μL, 2 mg mL−1) was dropped onto the well-polished bare GCE and then evaporated in air. Then, Nafion (5 μL, 2.5%) was dropped on the surface of $Co_3(PO_4)_2$ NRs to form a Nafion membrane ($Co_3(PO_4)_2$ NRs/GCE). A similar procedure was also applied to prepare the bulk $Co_3(PO_4)_2$/GCE for further experiments.

2.5. Apparatus and characterization

Powder X-ray diffraction (XRD) patterns were obtained with a XRD-7000 (XRD, Shimadzu XRD-7000) with Cu Kα source radiation at a scanning rate of 2 °min^{-1} from 10° to 80°. The surface properties of the samples were analyzed by X-ray photoelectron spectroscopy (XPS, Escalab 250xi, Thermo Scientific). The morphologies and structures were characterized by field-emission scanning electron microscopy (FESEM, JEOL-7800F), and transmission electron microscope (TEM, JEM-2100). The Brunauer–Emmett–Teller (BET) surface area was measured by using a Quadrasorb evo 2QDS-MP-30 (Quantachrome Instruments, USA) using nitrogen as the adsorption gas. Cells images and cell cultures were acquired with an inverted microscope (IX-71, Olympus Corp, Japan). The electrochemical measurements were carried out on a conventional three electrode system with the as-prepared electrodes as the working electrode, a platinum wire as the counter electrode, and a saturated calomel electrode (SCE) as the reference electrode on a CHI660 electrochemical workstation (CHI Instruments Inc).

2.6. Cell Cultures and real time monitoring cell released $O_2^{\bullet-}$ molecules

Hacat (spontaneously immortalized human keratinocyte) cell line was cultured in Dulbecco's modified Eagle's medium (DMEM) (Cellgro, USA) supplemented with 10% heat inactivated fetal bovine serum (Cellgro, USA), 1 mol L^{-1} glutamine (Beijing Dingguo Changsheng Biotech CO. LTD, China) and 50 U mL^{-1} penicillin/streptomycin (Cellgro, USA). A375 (human malignant melanoma cells) cell line was cultured in RPMI-1640 medium supplemented with 10% heat inactivated fetal bovine serum, 1 mol L^{-1} ampicillin and 1 mol L^{-1} kanamycin. These two cell lines were grown in a humidified incubator (95% air with 5% CO_2) at 37 °C. The cell density applied to our experiments was the average cell number counted from 6 different areas of 1.8 mm^2 on three samples through inverted microscopy. Real time monitoring $O_2^{\bullet-}$ molecules released from cells was performed by chronoamperometry. In order to ensure accuracy of measured $O_2^{\bullet-}$ concentrations, cell culture medium inside device was mildly stirred during cell released $O_2^{\bullet-}$ measurement.

3. Results and discussion

3.1. Characterization of materials

The crystal structure and phase purity of the $Co_3(PO_4)_2$ NRs obtained via the micro-emulsion method was first investigated using X-ray diffraction (XRD). As shown in Fig. 1a, where all of the diffraction peaks can be indexed to a $Co_3(PO_4)_2$ phase (JCPDS No. 13–0503), indicating high purity and crystallinity. Further structural details and compositions of the obtained $Co_3(PO_4)_2$ NRs were explored by X-ray photoelectron spectroscopy (XPS) analysis. In the wide scan survey XPS spectra of $Co_3(PO_4)_2$ NRs (Fig. 1b), many elements could be detected such as Co 2p (798.2 eV, 782.7 eV), O 1s (532.0 eV), P 2s (191.2 eV) and P 2p (134.0 eV). The Co 2p XPS spectra in Fig. 1c exhibited two major peaks at 782.7 and 798.2 eV, corresponding to Co $2p_{3/2}$ and Co $2p_{1/2}$, respectively. The spin-energy separation between the peak of Co $2p_{3/2}$ and the peak of Co $2p_{1/2}$ is approximately at 15.5 eV, which was characteristic of divalent cobalt (Chen et al., 2012). Typical XPS survey spectra of P 2s (191.2 eV) and P 2p (134.0 eV) emission peaks was presented in Fig. 1d, which was assigned to PO_4^{3-} (Hu et al., 2015). These results were consistent with those of the XRD results, indicating successful synthesis of $Co_3(PO_4)_2$..

The microstructure and morphology of the obtained $Co_3(PO_4)_2$ NRs were characterized with field-emission scanning electron microscopy (FESEM), transmission electron microscope (TEM), A typical FESEM image in Fig. 2a showed the clavate morphology of the products with a homogeneous size distribution of ~70 nm (Fig. 2b). The magnified FESEM image (Fig. 2c) of a few $Co_3(PO_4)_2$ nanorods revealed that it was composed of a large number of very tiny nanoparticles with diameters of ~16 nm (Fig. 2d). The TEM images (Fig. 2e and f) further confirmed their nanoporous structure and homogenous framework nature. The high magnification HRTEM image in Fig. 2g showed a clear atomic site array with an inter-planar spacing of 0.334 nm, which corresponded to the (2 1 0) lattice spacing of $Co_3(PO_4)_2$..

Generally, the products formed in micro-emulsion system were nanoparticles or nanospheres due to the limited growing space in the micro-emulsion droplets. Then $Co_3(PO_4)_2$ nanorods were observed in our work. In order to fully understanding the nucleation and crystal growth process of the unique $Co_3(PO_4)_2$ super-structures, we carefully investigated the effect of reaction condition (water solution or micro-emulsion droplets) and surfactants on the microstructure of products. As expected that the $Co_3(PO_4)_2$ formed in the $CoCl_2$ and K_3PO_4 mixed aqueous solution displayed big lamellar morphology (Fig. 3a). In

micro-emulsion system, the products were consisted of a large number of nanoparticles under low concentration surfactant. With the increasing of surfactant concentration, the morphologies of $Co_3(PO_4)_2$ nanorods (Fig. 3b to d) were observed gradually. The whole morphology evolution could be summarized in Fig. 3e. Based on above results and the literature reported before (Mitchell and Ninham, 1981), we believe that the Geometry theory and oriented growth process should be responsible for the final morphology forming process. In micro-emulsions system, the addition of surfactants could stabilize the micro-emulsions and control the microemulsion size. At a low concentration, the small microemulsion size is exactly used for nucleation and leading a large number of nanoparticles. With the increase of surfactant, the microemulsion size is large enough for the oriented growth towards the unique direction. Hence, not only small nanoparticles but also nano-architectures was highly available through the micro-emulsion method presented here..

The specific surface area and pore size distribution of the prepared samples were assessed based on N_2 adsorption/desorption measurements, and the results were displayed in Fig. 4a. Compared to bulk $Co_3(PO_4)_2$, the recorded adsorption and desorption isotherm of the $Co_3(PO_4)_2$ NRs exhibited a significant hysteresis at (P/P_0)=0.9 to 0.95, which might be ascribed to the inter-nanoparticles spacing. The peak of the pore size distribution calculated by Barrett-Joyner-Halenda (BJH) was located at 2 nm and was attributed to the packing of nanoparticles (Fig. 4b). The Brunauer-Emmett-Teller (BET) surface area of the $Co_3(PO_4)_2$ NRs (ca. 143.891 $m^2 g^{-1}$) calculated from the linear part was much bigger than that of bulk $Co_3(PO_4)_2$ (ca. 34.382 $m^2 g^{-1}$), and was attributed to the porosity and nanoscale structure of $Co_3(PO_4)_2$ NRs samples, as has been seen in the TEM images. These results further demonstrated the above synthesis strategy is an effective method for the synthesis of the material with large specific surface area and porous nature..

3.2. Electrochemical behaviors

The electrocatalytic activities of the prepared bulk $Co_3(PO_4)_2$ and $Co_3(PO_4)_2$ NRs towards superoxide anion were studied using cyclic voltammograms (CVs). As shown in Fig. 5a, each prepared electrode exhibited a sharp oxidative peak and reductive wave, which could be assigned to the electrochemical transformation between Co(II) and Co(III). Compared to the bulk $Co_3(PO_4)_2$ based electrode, a remarkable increase in the anodic current was observed for $Co_3(PO_4)_2$ NRs based electrodes after the addition of $O_2^{\bullet-}$ solution, demonstrating superior electrocatalytic activity and kinetic process towards $O_2^{\bullet-}$ oxidation, which was mainly attributed to the high electrochemical ability, large specific surface area, rich porous network, and lower reaction and diffusion resistance of $Co_3(PO_4)_2$ NRs..

In order to further investigate the possibility of the prepared $Co_3(PO_4)_2$ NRs as biomimetic enzymes, the fabricated electrodes was employed as biosensors for detecting $O_2^{\bullet-}$. Typical stepwise current response with increasing $O_2^{\bullet-}$ concentration under stirring at an applied potential of 0.7 V in 10 mL 0.01 M pH 7.4 PBS was observed, in which 30 s wait between every step increase and 95% of the steady-state current was reached within 3 s (Fig. 5b). The corresponding calibration curve was presented in Fig. 5c. A linear response range was acquired from 5.76 to 5390 nM with a detection limit of 2.25 nM based on a signal-to-noise ratio (S/N=3), and the sensitivity is calculated to be 1.015×10^{-2} μA/nM (the linear fitting correction coefficient R^2=0.999).

The specificity and reproducibility are two important variables when monitoring $O_2^{\bullet-}$ in biological systems. The anti-interference performance towards ions and other small molecules, which are possibly oxidized along with $O_2^{\bullet-}$ on the electrode surface to cause interfering electrochemical signals, is one of the biggest concerns for electrochemical sensors. Thus, it is essential to investigate the effects of interferences on the current response of the sensing materials for $O_2^{\bullet-}$ oxidation. As seen in Fig. 5d, the presence of K^+, Na^+, Cl^-, SO_4^-, NO_3^-, AA, UA, NO as well as H_2O_2 did not cause any noticeable interference in response to 1.01×10^{-6} M $O_2^{\bullet-}$. The observed excellent selectivity was presumably due to the specific catalytic effect of the biomimetic superoxide dismutase $Co_3(PO_4)_2$ NRs to $O_2^{\bullet-}$. The reproducibility of the developed sensor was also tested using three different electrodes. The relative standard deviations (RSD) of the current responses for $O_2^{\bullet-}$ were less than 2.2%. These results showed that the $Co_3(PO_4)_2$ NRs -based sensors possess acceptable specificity and reproducibility for analytical applications.

As a biomimetic enzyme, $Co_3(PO_4)_2$ NRa/GC electrode was further applied to in situ detect $O_2^{\bullet-}$ released from two cell lines, including HaCat spontaneously immortalized human keratinocyte cells and A375 human malignant melanoma cells. Zymosan was chosen as the functional drug to stimulate living cells to release molecular $O_2^{\bullet-}$. Detailed investigation of the dynamic responses of HaCat cells with a cell density of 5×10^4 mL^{-1} were presented in Fig. 6a. The stimulating agent was continuously injected under mild stirring, as indicated by the arrow. As soon as 2 g L^{-1} (curve a) or 1 g L^{-1} (curve b) Zymosan was added into the cell culture medium, a significant current response appeared, corresponding to $O_2^{\bullet-}$ oxidation. It was pertinent to mention that the sensing is an in situ detection since the GCE sensor directly detected $O_2^{\bullet-}$ released from a number of cells in contact with the electrode surface. In contrast, a mixture of 1 g L^{-1} Zymosan and SOD 300 U mL^{-1} (curve c) did not cause any obvious step increases, indicating that the released $O_2^{\bullet-}$ molecules were consumed by SOD. Furthermore, the calculated concentrations of $O_2^{\bullet-}$ released from HaCat cells were around 215.18 nM and 108.69 nM with the addition of 2 g L^{-1} and 1 g L^{-1} Zymosan, respectively, according to the drug-stimulated current response and calibration equation for the $Co_3(PO_4)_2$ NRa/GC electrode sensor. Control experiments showed that no current was obtained in the culture medium upon the addition of either Zymosan or Zymosan-SOD mixture (curve d), confirming that the current responses were attributed to the drug-induced $O_2^{\bullet-}$ release from HaCat cells. The current response caused by the addition of 2 g L^{-1} Zymosan drug was about 1.97 times than that of 1 g L^{-1} Zymosan, suggesting that the response under Zymosan stimulation was a concentration-dependent behavior..

Moreover, similar responses of the $Co_3(PO_4)_2$ NRa/GC electrode sensor to A375 cells with a cell density of 5×10^4 mL^{-1} are presented in Fig. 6b. However, the current step intensity obtained with A375 cells was much weaker (ca. 10%) than that with HaCat cells, indicating less $O_2^{\bullet-}$ released by A375 cells upon the same drug stimulation.

4. Conclusions

In conclusion, $Co_3(PO_4)_2$ NRs with high surface area and porous slack structure has been successfully synthesized via a simple and effective micro-emulsion method followed by high temperature calcination. And we found that not only small nanoparticles but also some unique super-architectures was highly available through designed micro-emulsion system. As a nanostructured biomimetic enzyme, the as-synthesized $Co_3(PO_4)_2$ NRs performs exceptionally toward the catalysis of $O_2^{\bullet-}$ offering high sensitivity, wide linear range, low detection limit, excellent specificity and good reproducibility in detection of $O_2^{\bullet-}$ by the rationally designed sensor architecture. In particular, in situ monitoring of $O_2^{\bullet-}$ released from cells under drug stimulation is accomplished with our biosensor, showing great capability for real time and sensitive quantitative detection. It is concluded that this biomimetic enzyme render much higher durability than natural ones, thus suggesting great promise for broad application in fundamental research, clinic diagnostics, and screening for drug therapy effects.

Note

The authors declare no competing financial interest.

Acknowledgements

This work is financially supported by National Natural Science Foundation of China (21163021, 21375108); Chongqing Key Laboratory for Advanced Materials and Technologies of Clean Energies, and Program for Excellent Talents in Chongqing (102060-20600218). Minqiang Wang and Cui Ye contributed equally to this work.

References

Ahmad, J., Alhadlaq, H.A., Siddiqui, M.A., Saquib, Q., Al-Khedhairy, A.A., Musarrat, J., Ahamed, M., 2015. Environ. Toxicol. 30 (2), 137–148.
Anacona, J.R., Azocar, M., Nusetti, O., Rodriguez-Barbarin, C., 2003. Transit. Met. Chem. 28 (1), 24–28.
Arico, A.S., Bruce, P., Scrosati, B., Tarascon, J.-M., Van Schalkwijk, W., 2005. Nat. Mater. 4 (5), 366–377.
Barnese, K., Gralla, E.B., Cabelli, D.E., Selverstone Valentine, J., 2008. J. Am. Chem Soc. 130 (14), 4604–4606.
Boakye, E., Radovic, L.R., Osseo-Asare, K., 1994. J. Colloid Int. Sci. 163 (1), 120–129.
Cheetham, A.K., Férey, G., Loiseau, T., 1999. Angew. Chem Int. Ed. 38 (22), 3268–3292.
Chen, B.D., Peng, C.X., Zheng, C., 2012. T Nonferr. Met. Soc. 22 (10), 2517–2522.
Dai, Z., Liu, S., Bao, J., Ju, H., 2009. Chem. Eur. J. 15 (17), 4321–4326.
Di, J., Bi, S., Zhang, M., 2004. Biosens. Bioelectron. 19 (11), 1479–1486.
Diez, L., Livertoux, M.-H., Stark, A.-A., Wellman-Rousseau, M., Leroy, P., 2001. J. Chromatogr. B 763 (1), 185–193.
Durot, S., Policar, C., Cisnetti, F., Lambert, F., Renault, J.P., Pelosi, G., Blain, G., Korri-Youssoufi, H., Mahy, J.P., 2005. Eur. J. Inorg. Chem. 2005 (17), 3513–3523.
Entezari, M.H., Ghows, N., 2011. Ultrason. Sonochem. 18 (1), 127–134.
Feng, P., Bu, X., Tolbert, S.H., Stucky, G.D., 1997. J. Am. Chem. Soc. 119 (10), 2497–2504.
Fitzgerald, A., Osman, A., Xie, T., Patel, A., Skinner, H., Sandulache, V., Myers, J., 2015. Cell Death Dis. 6 (3), 1678–1687.
Garrou, P.E., 1985. Chem. Rev. 85 (3), 171–185.
Hu, F.X., Kang, Y.J., Du, F., Zhu, L., Xue, Y.H., Chen, T., Dai, L.M., Li, C.M., 2015. Adv. Funct. Mater. 25 (37), 5924–5932.
Husein, M.M., Rodil, E., Vera, J.H., 2007. J. Nanopart. Res. 9 (5), 787–796.
Ignatov, S., Shishniashvili, D., Ge, B., Scheller, F.W., Lisdat, F., 2002. Biosens. Bioelectron. 17 (3), 191–199.
Knowles, J.C., 2003. J. Mater. Chem. 13 (10), 2395–2401.
Liao, S.-H., Lu, S.-Y., Bao, S.-J., Yu, Y.-N., Wang, M.-Q., 2016. Anal. Chim. Acta 905, 72–78.
Long, R., Huang, H., Li, Y., Song, L., Xiong, Y., 2015. Adv. Mater. 27 (44), 7025–7042.
Mitchell, D.J., Ninham, B.W., 1981. J. Chem. Soc. Faraday Trans. 77 (4), 601–629.
Natarajan, S., Neeraj, S., Choudhury, A., Rao, C.N.R., 2000. Inorg. Chem. 39 (7), 1426–1433.
Ohara, Y., Peterson, T.E., Harrison, D.G., 1993. J. Clin. Invest. 91 (6), 2546–2551.
Pierre, J.-l, Chautemps, P., Refaif, S., Beguin, C., El Marzouki, A., Serratrice, G., Saint-Aman, E., Rey, P., 1995. J. Am. Chem. Soc. 117 (7), 1965–1973.
Salvemini, D., Muscoli, C., Riley, D.P., Cuzzocrea, S., 2002. Pulm. Pharm. Ther. 15 (5), 439–447.
Tian, Y., Mao, L., Okajima, T., Ohsaka, T., 2002. Anal. Chem. 74 (10), 2428–2434.
Tilley, R.D., Warner, J.H., Yamamoto, K., Matsui, I., Fujimori, H., 2005. Chem. Commun. 14 (14), 1833–1835.
Vásquez-Vivar, J., Kalyanaraman, B., Martásek, P., Hogg, N., Masters, B.S.S., Karoui, H., Tordo, P., Pritchard, K.A., 1998. Proc. Natl. Acad. Sci. 95 (16), 9220–9225.
Wang, M.-Q., Ye, C., Bao, S.-J., Zhang, Y., Yu, Y.-N., Xu, M.-w, 2016a. Analyst 141, 1279–1285.
Wang, M.-Q., Zhang, Y., Bao, S.-J., Yu, Y.-N., Ye, C., 2016b. Electro. Acta 190, 365–370.
Ye, C., Wang, M.Q., Zhong, X., Chen, S., Chai, Y., Yuan, R., 2015. Biosens. Bioelectron. 79, 34–40.
Zhang, L., Tang, B., Ding, Y., 2005. J. Agr. Food Chem. 53 (3), 549–553.
Zhou, Y., Ding, J., Liang, T., Abdel-Halim, E., Jiang, L.-P., Zhu, J.-J., 2016. ACS Appl Mater. Int. 8 (10), 6423–6430.
Zweier, J.L., Flaherty, J.T., Weisfeldt, M.L., 1987. Proc. Natl. Acad. Sci. 84 (5), 1404–1407.